








Power-to-Frequency Dependency of Residential Loads in a Wider Frequency Range: An Experimental Investigation

Johanna Geis-Schroer *, Student Member, IEEE, Qiucen Tao *, Student Member, IEEE, Maëva Courcelle , Student Member, IEEE, Gregor Bock , Michael Suriyah , Member, IEEE, Thomas Leibfried , Senior Member, IEEE, and Giovanni De Carne , Senior Member, IEEE

* These authors contributed equally to this work.

Abstract—With decreasing rotational inertia from traditional synchronous generation, frequency is becoming more volatile. Hence, a closer assessment of frequency-dependent load behavior is required. This paper presents an experimental investigation for residential loads, including sixteen typical domestic appliances. The perturbation-based method (range 50 ± 1 Hz) is applied to determine frequency sensitivity values as parameters for commonly used exponential and linear frequency-dependent load models. Subsequently, these models with their identified parameters are compared with the measured load behavior of four representative devices during dynamic and steady-state frequency variations. The comparison shows a significant increase in the reconstruction error beyond the 50 ± 1 Hz range, which suggests that the model parameters identified for a small frequency range may not be the most effective for larger frequency variations. The experimental study presented in this paper also includes a PV inverter as a representative of the increasing number of distributed generator and storage systems. The frequency-dependent behavior of such systems is defined in grid codes in some countries (e.g. VDE-AR-N 4105 in Germany). The measured response from the PV inverter under test shows that there is a non-negligible response delay time, and thus modeling approaches must be upgraded in the future.

Index Terms—Load modeling, frequency sensitivity, demand response, distributed generators, perturbation-based sensitivity identification method.

I. INTRODUCTION

AS in most power grids worldwide, a transition from traditional synchronous generation towards power electronic-based generation from renewable resources is occurring in the Continental European power system. As a consequence, the amount of rotational inertia present in the grid is decreasing, which makes frequency control more challenging and results in larger frequency excursions after power imbalances [1]. In smaller isolated systems, e.g. on remote islands, the amount of inertia has always been limited [2], [3]. Hence, already today, it is not uncommon that loads experience larger frequency fluctuations in such systems. The difference in frequency volatility to be expected depending on the extension of a power grid is specified

This work was supported by the Helmholtz Association under the program "Energy System Design". The work of Giovanni De Carne, Qiucen Tao, and Maëva Courcelle was supported by the Helmholtz Association within the Helmholtz Young Investigator Group "Hybrid Networks" (VH-NG-1613).

in the European power quality standard EN 50160 [4]. In interconnected systems such as Continental Europe, the 10-second average of the frequency must always remain between 47 Hz and 52 Hz. In contrast, for isolated systems, temporary deviations of ± 7.5 Hz still meet the standard. The review on grid code requirements in [5] shows that some grid operators actually make use of the less restrictive limits defined in EN 50160. Fig. 1 contrasts the generator withstand capability requirements of exemplary isolated systems with those of Continental Europe. The widest is specified for French Guiana, where generators must be able to operate in the range 44 Hz to 55 Hz.

Although increasing inertia-related frequency control concerns in most power systems worldwide further highlight the need for a closer assessment of frequency-dependent load behavior, a surprisingly low number of studies on this topic is available in the literature. The importance of accurate load representation has been acknowledged since the 1930s [6]–[8]. However, the majority of the existing research in this area has predominantly focused on the relationship between voltage and power, often overlooking the impact of frequency [9]–[14]. This is usually due to the assumption that frequency remains relatively stable around its nominal value compared to voltage, particularly in large interconnected power systems [15].

Furthermore, existing frequency-dependent load models use simple exponential or linear functions to characterize frequency dependency [15]. The effectiveness of these functions in a wide frequency range (50 ± 6 Hz) remains unverified. With the experimental study presented in this

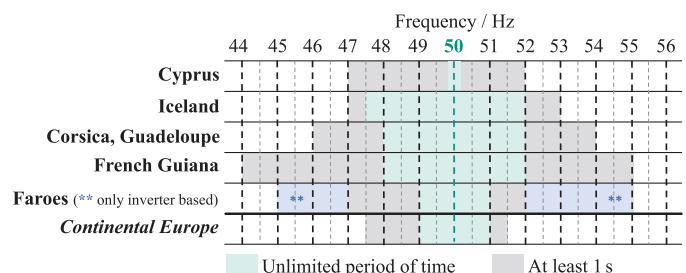


Fig. 1. Generator withstand capability requirements in different European power systems, based on [5].

paper, we aim to conduct a preliminary verification using actual measurements from modern residential loads. In case of the German power system, about 25 % of the total power consumption is attributed to residential loads, which makes them one of the largest consumers in the country [16]. It should be emphasized that in this paper, the term "residential loads" does not solely comprise domestic appliances such as refrigerators or washing machines, but also distributed generators such as rooftop photovoltaic (PV), or energy storage systems. This is a typical case for the German grid, where the number of currently installed rooftop PV systems is estimated to be about two million (as of 2021 [17], [18]).

Recently, a number of works have discussed the possibility of enhancing power controllability of low voltage grids by using power electronics for frequency control that targets the frequency dependency of residential loads [19], [20]. To further assess the potential of this approach, a clear understanding of the behavior of different types of loads during large frequency fluctuations is required.

Similar to the experiments conducted in this work, [21] in 1998 experimentally studied the frequency dependency of loads in the range 60 ± 6 Hz. However, only lighting loads and the composite load of office equipment were tested, and this data is now outdated. The most recent comprehensive overview of currently used load models and their respective parameters was presented in 2014 and 2018 by CIGRE Working Group C4.605 [22], [23]. However, the frequency dependency parameters reported are predominantly based on data from the 1970s and 1980s [8], [24], [25], and are also outdated. Over the last few decades, there have been significant changes in the technologies used in loads, particularly with the increased adoption of power electronic-based devices. The CIGRE report reveals the need for a more recent update of frequency dependency parameters. In this paper, we aim to introduce the following contributions regarding the frequency-dependent behavior of modern residential loads:

- Updated frequency sensitivity values for sixteen commercial domestic devices, obtained with the novel perturbation-based method (range 50 ± 1 Hz), to be applied for linear and exponential load modeling approaches; partially already presented in [26], an earlier conference version of this work.
- Measurements of the power response of selected devices under frequency variations in the range 50 ± 6 Hz (a notably wide range compared to existing studies); both during steady-state and trapezoidal dynamic variations.
- Comparison and analysis of the suitability of currently used frequency-dependent load models (linear and exponential) for a wider frequency range.
- Investigation into the behavior of a real PV inverter: analysis of the delay time for power adjustment when the inverter is exposed to frequency disturbances with different Rate of Change of Frequency (RoCoF).

The rest of the paper is structured as follows: In Section II, we explain the frequency-dependent load models, and the methodology used in this work to investigate the power-to-frequency dependency of domestic appliances. The

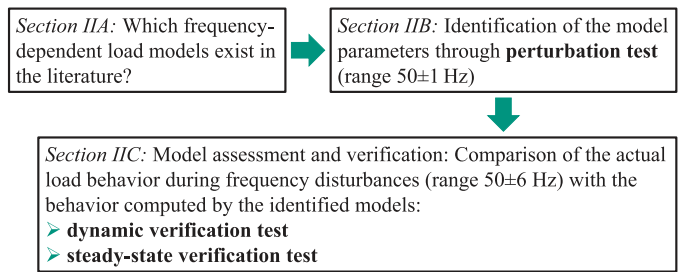


Fig. 2. Concept figure to explain methodology.

experimental setup and the loads under test are presented in Section III. Results on the frequency dependency of domestic appliances are discussed in Section IV, whereas Section V provides insights into the frequency-dependent behavior of a PV inverter. Finally, conclusions are drawn in Section VI.

II. METHODOLOGY

The outline of this section aligns with the methodology concept illustrated in Fig. 2. First, the theoretical background of frequency-dependent load models is presented (Section II-A). The following sections introduce the experimental and analytical methods used to identify frequency-dependent model parameters for the range 50 ± 1 Hz (II-B), and to assess the performance of the identified models along with their parameters in a wider frequency range (II-C).

A. Frequency-Dependent Load Models

Based on survey replies received from 97 industrial participants all over the world, it is reported in [22] that about 70 % of utilities and system operators only use static load models—both for static and dynamic power system stability studies. Hence, we focus on these commonly used models in this work. Static load models express the active and reactive power consumed by a load as simple functions of the voltage magnitude and frequency at the load bus. Differences in load models in the literature predominantly lie in the representation of voltage dependency [15].

Static load models that include frequency dependency are derived by multiplying the voltage-dependent term with a frequency-dependent term, usually either in the exponential or linear form [15]. If operation at nominal voltage is assumed and only the frequency-dependent term is considered, the exponential frequency-dependent model (in short, exponential model) can be mathematically expressed as (1). If the frequency variation is relatively small (typical for large interconnected systems), a first-order Taylor series approximation of the exponential model can be used. This approximation generates the well-known linear frequency-dependent model (in short, linear model), expressed as (2).

$$P_{\text{exp}}(f) = P_0 \cdot \left(\frac{f}{f_0} \right)^{K_{pf}} \quad (1)$$

$$P_{\text{lin}}(f) = P_0 \cdot \left(1 + K_{pf} \frac{f - f_0}{f_0} \right) \quad (2)$$

In (1) and (2), f_0 is the rated frequency (not necessarily the nominal frequency), P_0 is the active power at the rated frequency, and K_{pf} represents the active power-to-frequency sensitivity. With Q_0 as reactive power at the rated frequency and K_{qf} as reactive power-to-frequency sensitivity, the same equations apply to the reactive power-to-frequency models $Q_{\text{exp}}(f)$ and $Q_{\text{lin}}(f)$. Since the frequency sensitivity is the relative change in power with respect to a change in frequency, it can be mathematically defined as (3) and (4) for active and reactive power, respectively.

$$K_{pf} = \left. \frac{dP/P_0}{df/f_0} \right|_{f=f_0} \quad (3)$$

$$K_{qf} = \left. \frac{dQ/Q_0}{df/f_0} \right|_{f=f_0} \quad (4)$$

It should be noted that the frequency sensitivity is a rated value, and the rated point (f_0, P_0) or (f_0, Q_0) should always be specified. As demonstrated in [27], the rated point (f_0, P_0) is not necessarily the nominal power at nominal frequency, but can be any operating point (f_k, P_k) as long as $(P_0/f_0)^{K_{pf}} = (P_k/f_k)^{K_{pf}}$. Therefore, (3) and (4) can be discretized, and the frequency sensitivity can be calculated as below:

$$K_{pf} = \left. \frac{dP/P_k}{df/f_k} \right|_{f=f_k} \approx \frac{(P_k - P_{k-1})/P_k}{(f_k - f_{k-1})/f_k} \quad (5)$$

$$K_{qf} = \left. \frac{dQ/Q_k}{df/f_k} \right|_{f=f_k} \approx \frac{(Q_k - Q_{k-1})/Q_k}{(f_k - f_{k-1})/f_k} \quad (6)$$

In the discretized version of the frequency sensitivity, the subscript k denotes the current calculation step, and the subscript $k-1$ denotes the previous calculation step. Following these calculations, it can be concluded that the frequency sensitivity provides the ratio of the percentage of active or reactive power variation to the percentage of frequency variation. For instance, K_{pf} equal to -2 indicates an active power reduction of 2% if the frequency increases by 1%.

B. Frequency Sensitivity Identification with the Perturbation-Based Method

The exponential and the linear model, as presented in (1) and (2), each have one single unknown parameter: the frequency sensitivity (K_{pf} or K_{qf}). To determine these model parameters for residential appliances, we applied the perturbation-based approach. Initially introduced in [27], this method allows for the experimental determination of frequency sensitivity by inducing minor artificial frequency fluctuations and concurrently monitoring the power response of the loads.

As illustrated in Fig. 3 (top subplot), we used a sinusoidal frequency disturbance in this work. The disturbance signal has a period of 1.25s and an amplitude of 1 Hz. It is not applied to the loads continuously but is activated every 15 s for 4 periods (5 s). The power response is recorded (middle subplot) to compute the frequency sensitivity using (5) and (6). The sensitivity (bottom subplot) is calculated consistently during the 5 s (in black), and the average value over the 5 s is taken as the final result for that disturbance (in red). The frequency and power average over 1 s before the disturbance—marked in red in the top and middle subplots in Fig. 3—is used

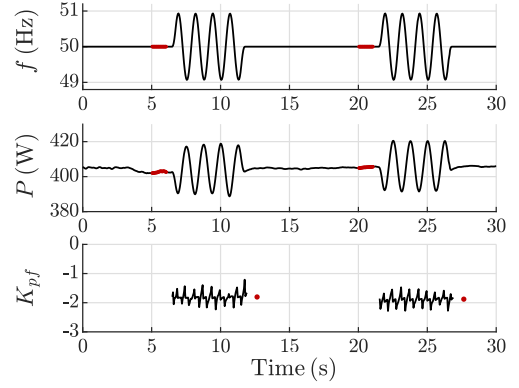


Fig. 3. Example of a perturbation-based sensitivity identification approach: apply a frequency disturbance and measure the power response.

as the rated point. In the remainder of this paper, we will refer to this test scenario as **perturbation test**.

Due to limited power meter accuracy and increased noise influence, the accuracy of the identified frequency sensitivity is reduced for low power consumption. However, the influence of such low-power loads on the system is minimal, making precision enhancement at low power a secondary priority for this study. Here, frequency sensitivity for power below 20 W or 20 var was therefore not calculated, and the value was assumed to be zero. It is worth noting that we only considered power fluctuations directly attributable to provoked frequency changes. Large power variations resulting from operational state changes or measurement noise were excluded from the analysis.

C. Model Assessment and Verification in the Range 50 ± 6 Hz

The frequency sensitivity K_{pf} , identified through the perturbation test as explained in Section II-B, can be used as model parameter for the exponential and the linear model. Theoretically, we can compute the active power consumed by a load at any supply frequency f by (1) or (2), assuming that the supply voltage remains constant and that the reference power P_0 is known. Similarly, we can use K_{qf} to calculate the frequency-dependent reactive power consumption.

Although the linearized form in (2) is used more often than the exponential model in (1), a frequency range for the validity of the linear model has never been established. Fig. 4 illustrates the relative mathematical error e_m (absolute value) between the two models for the frequency range 44–56 Hz and frequency sensitivity in the range 1–6. The error is calculated from (7), where P_{exp} and P_{lin} represent the active power calculated with the exponential model and the linear model, respectively, if both models use the same K_{pf} value. The same relationship applies to the calculation of the reactive power Q_{exp} and Q_{lin} , if the same K_{qf} value is used.

$$e_m = \frac{|P_{\text{exp}} - P_{\text{lin}}|}{P_{\text{exp}}} \quad (7)$$

Fig. 4 demonstrates that a sensitivity of 1 causes no deviation between the two models. As the sensitivity increases, the error e_m becomes larger. For frequency variations in

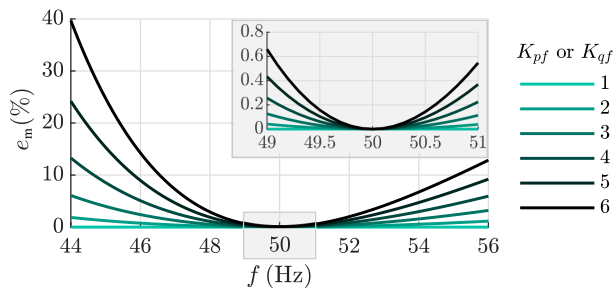


Fig. 4. Relative mathematical error between the exponential and the linear load model for 50 ± 6 Hz, when frequency sensitivity increases from 1 to 6.

the range 50 ± 1 Hz, it remains below 0.7%. In general, the error between the two models is more pronounced in the underfrequency range than in the overfrequency range. While the error reaches approx. 15% for a frequency deviation of +6 Hz, it reaches approx. 40% for -6 Hz. Fig. 4 suggests that—at least from a mathematical point of view—there is some limitation in using the linear model. Thus, it is necessary to investigate which model is more suitable to describe the behavior of loads over a wider frequency range.

To assess the model performance in the range 50 ± 6 Hz, we exposed selected loads to two different test scenarios:

Dynamic verification test Trapezoidal variation with ramps of ± 1 Hz/s and absolute deviations of ± 6 Hz.

Steady-state verification test Steady-state deviations in the range 50 ± 6 Hz in steps of 1 Hz, with a duration of 90 s for each step.

For the results presented in Section IV, the measured power profiles are compared with the power profiles that would be calculated by the models. For each measurement sample at time t , the relative reconstruction error—here indicated for active power—is calculated from (8).

$$e_{rec,t} = \frac{P_{rec,t} - P_{meas,t}}{P_{meas,t}} \quad (8)$$

In (8), $P_{meas,t}$ is the measured power at time t . $P_{rec,t}$ is the reconstructed power, i.e. the power computed by one of the models using the previously identified sensitivity and the frequency f at time t as input. If $e_{rec,t}$ is positive, the reconstruction overestimates the power consumption at time t .

III. EXPERIMENTAL SETUP AND LOADS UNDER TEST

This section explains how the methods introduced in Section II were applied to modern domestic loads. It should be remarked that this section focuses solely on tests performed with domestic appliances. Explanations regarding the PV inverter tests will be provided in Section V.

The experimental investigation was performed under realistic household conditions at the Energy Smart Home Lab (ESHL) which is located on the Campus South of *Karlsruhe Institute of Technology (KIT)*. The ESHL is a 60 m² two-bedroom apartment with typical domestic appliances and several distributed generation and storage units. All devices have been installed within the last 15 years, and thus represent a common set of equipment for apartments. The

TABLE I
DOMESTIC APPLIANCES UNDER TEST.

Appliance	Brand and Model	Tested Operating Mode
Oven	Miele H5681BL	Top and bottom heating, set temperature 280° C
Water kettle	Clatronic WKS 3692	Cook 1.5L water
Induction stove	Miele KM 5955	Maximum power level of a single plate
Condenser dryer	Miele T 8687 C	Gentle cycle
Microwave oven	Renkforce MM720CA7-PM	Maximum power level
Dishwasher	Miele G 1834 SCI	Quick wash 40° C
Toaster	Severin AT 2586L	Maximum power level
Halogen ceiling lights ^a	- ^b	Lights on
Washing machine	Miele 3985 WPS	Cotton wash 1000 rpm
Vacuum cleaner	Siemens VBBS607V00	Smooth surface cleaning
Cooker hood	- ^b	Medium extraction level
LED TV screen	LG 75UM7110PLB	Display a white screen
Electric shutter	- ^b	Moving up-/downwards
Fan	CasaFan SPEED 50 G	Maximum power level
Freezer	Liebherr GN 3056-29	Cooling phase, set temperature -20° C
Refrigerator	Bosch KG KIRR18A	Cooling phase, set temperature 4° C

^a A light set contains 32 tubes.

^b No information available.

entire apartment can be disconnected from the public low-voltage grid and connected as hardware under test to a power hardware-in-the-loop environment [28].

Fig. 5 illustrates the setup used for the experiments, which allows us to expose the loads installed in ESHL to artificial frequency variations which would not occur under standard grid conditions. The ESHL is supplied by a three-phase four-quadrant linear voltage amplifier (type PAS 30000 by Spitzenberger & Spies). An OPAL-RT real-time simulator provides control signals to the voltage amplifier. Since the focus of this work is to analyze the power response of loads to frequency variations, the phase voltage Root Mean Square (RMS) values were actively controlled to maintain them at 230 V. To allow for voltage drop compensation across the 100-meter power cable, the voltage measured at ESHL is fed back to the amplifier sense inputs through a sense cable. Measurements of voltage RMS, current RMS and power values are performed with a cycle time of 50 ms using the precision power analyzer LMG450 by ZES Zimmer and its corresponding current clamps.

The ESHL fuse box allows us to connect and disconnect individual devices. To distinguish the behavior of individual loads, only one device per phase at a time was connected to the amplifier during the experiments. The loads selected for the experiments comprise sixteen conventional domestic appliances. Table I gives an overview of the brand, model, and tested operating mode of each device. The appliances differ in technology, and range from ac-to-dc power adapters to motor-based appliances (e.g. fan or washing machine), lights, and mainly resistive loads (e.g. water kettle). To achieve maximum test repeatability, a "constant" load behavior was chosen whenever possible. For instance, the LED TV screen was made to display a white screen instead of moving images.

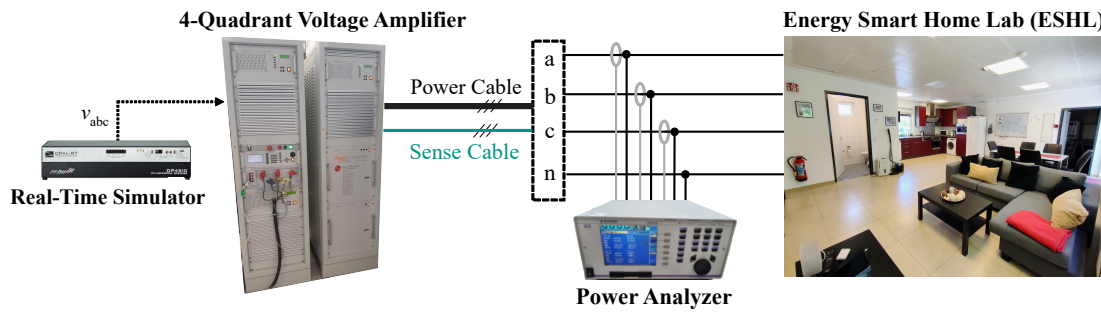


Fig. 5. Experimental setup with the Energy Smart Home Lab as hardware under test.

IV. EXPERIMENTAL RESULTS FOR CONVENTIONAL DOMESTIC APPLIANCES

In this section, we demonstrate experimental results on the frequency dependency of common domestic appliances, obtained with the methods explained in Section II and the experimental setup described in Section III. First, Section IV-A presents the frequency sensitivity values identified through the perturbation test. Using the sensitivity values as model parameters, we show results from the steady-state and the dynamic verification test in Sections IV-B and IV-C. The results are compared and discussed in Section IV-D.

A. Frequency-Dependent Load Models Determined Through the Perturbation Test

In this section, we present the frequency sensitivity values identified with the perturbation-based method (see Section II-B) for 16 common residential loads. As specified in Table I, each load was tested under a realistic operating mode. During the operation, a frequency sensitivity value was calculated every 15 s, and the overall average was taken as the equivalent frequency sensitivity of the device.

An overview of the equivalent frequency sensitivity of the domestic appliances is provided in Fig. 6. Among the sixteen tested loads, nine show active power and/or reactive power-to-frequency dependency, with K_{pf} ranging from -1.8 to 1.5 , and K_{qf} from -3.1 to 6.6 . On the one hand, the condenser dryer, the vacuum cleaner, the cooker hood, the electric shutter, the fan, and the freezer are driven by different types of single-phase induction motors directly connected to the grid. The respective sensitivity values in Fig. 6 confirm that motor-based loads are sensitive to frequency. Inside the microwave, there is a high-voltage transformer, which also results in non-zero sensitivity values. However, thermal loads such as the oven, the water kettle, and the toaster show neither active nor reactive power-to-frequency sensitivity, as they consist mainly of resistors. The same can be observed for the refrigerator, a power electronic-interfaced device due to its variable-speed compressor. The induction stove and the LED TV screen show only reactive power-to-frequency dependency. These devices are also power electronic-interfaced, so active power is actively controlled. In these cases, it can be assumed that a large input capacitor may cause a positive K_{qf} .

It is worth noting that the sensitivity value is determined by the physical characteristics of the main operating components

of the device. Most residential loads have consistent operating components. If those devices are tested under other operating modes, their sensitivity values will not change significantly. A few devices show different physical characteristics in different working phases as the main operating component varies. A washing machine, for instance, is highly resistive in the water warm-up phase, but motor-based during the rest of the operation. However, changes in the operating mode cause only minor variations in the sensitivity average value, i.e. the equivalent sensitivity value. Therefore, the sensitivity values provided in Fig. 6 can be considered applicable beyond the specific tested operating mode indicated in Table I.

B. Dynamic Verification Test Results

In the previous section, the parameters (frequency sensitivity) of the linear and exponential load models of common residential appliances were determined within the range 50 ± 1 Hz. To assess if the models in combination with these parameters can be used to describe the load behavior in a wider frequency range (50 ± 6 Hz), we present results from the dynamic verification test in this section.

1) *Selected loads*: To minimize the impact of potential internal state changes on the power consumption, four devices with consistent operating components, and thus constant sensitivity values during the operation, were selected:

- *Vacuum cleaner (V)*: a representative of motor-based loads, also the load with the largest negative K_{pf} value.
- *Microwave (M)*: a representative of transformer-based loads, also the load with the largest negative K_{qf} value.
- *LED TV screen (L)*: a representative of power electronic-interfaced appliances, with K_{pf} equal to zero.
- *Fan (F)*: a representative of motor-based loads, and also the load with the largest positive K_{pf} value in Fig. 6.

2) *Measured and reconstructed profiles*: As introduced in Section II-C, the loads were exposed to trapezoidal frequency variations in the range 50–56 Hz (overfrequency test) and 50–44 Hz (underfrequency test). In Fig. 7, the underfrequency test curve is shown in the top subplot (black). To repeat the test, the trapezoidal variation was applied three times. In Fig. 7, the measured active power profile (P_{meas} , black) is compared to a reconstruction of the profile (P_{rec}) calculated from the exponential model (green dotted line) and the linear model (green dashed line), both using the respective K_{pf} value in Fig. 6. To observe the load behavior within the ± 1 Hz

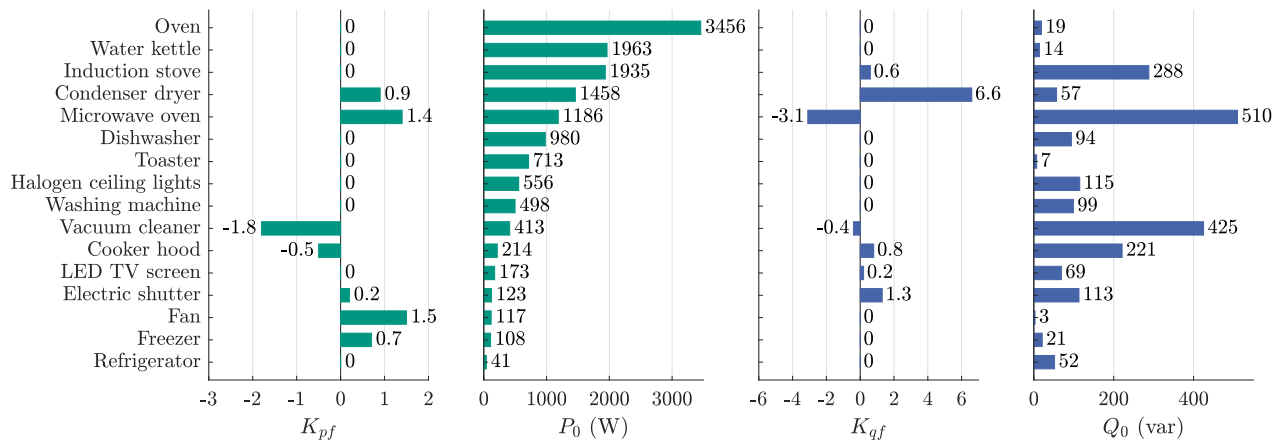


Fig. 6. Equivalent power-to-frequency sensitivity and corresponding rated power of the domestic appliances under test.

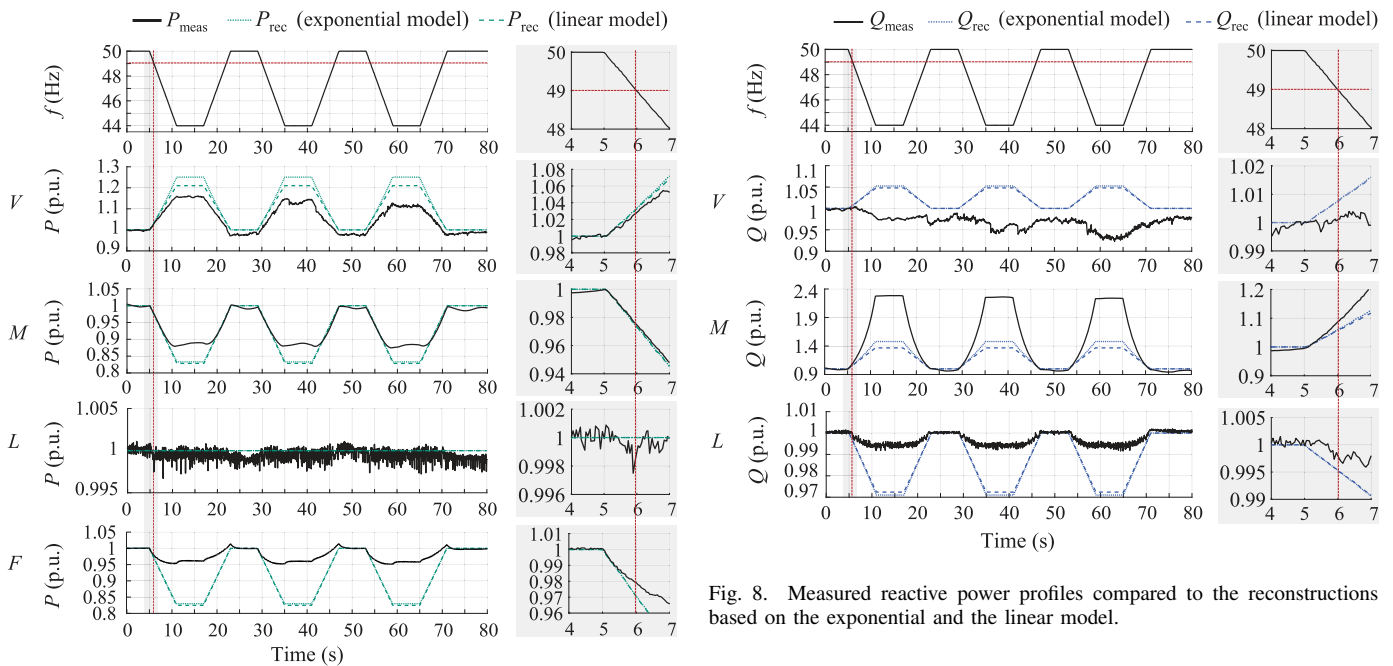


Fig. 7. Measured active power profiles compared to the reconstructions based on the exponential and the linear model.

Fig. 8. Measured reactive power profiles compared to the reconstructions based on the exponential and the linear model.

range better, zoomed plots of 50–48 Hz (gray background) are provided on the right side. In Fig. 8, the same is shown for the reactive power profiles. It should be mentioned that no plot is provided for the reactive power profile of the fan, since the reactive power consumption of the fan during the perturbation test (3 W in Fig. 6) was too low for an accurate determination of K_{qf} . Due to limitations of space, we do not provide figures for the overfrequency test.

3) *Normalization and reference values:* Although tested with the same operating modes, the measured power of the devices at 50 Hz slightly differed between the perturbation test and the dynamic verification test. This difficulty in replicating exactly the same load behavior may result from numerous factors such as differences in the ambient or the internal device temperature. To be able to compare the measured and the reconstructed behavior, we normalize the reconstructed power

using the rated power P_0 or Q_0 from Fig. 6, and the measured power by P_0^* or Q_0^* . These new reference values P_0^* and Q_0^* were calculated by averaging over the last 5 s before the first ramp starts, and are listed in Table II. In Fig. 7 and Fig. 8, power values are shown in per unit (p.u.).

4) *Evaluation of the reconstruction error:* We take the first ramp of the trapezoidal variation as an example for a quantitative evaluation of the reconstruction error in the ± 1 Hz range ($t \in [5, 6]$ s in Fig. 7 and Fig. 8) and the ± 6 Hz range ($t \in [5, 11]$ s), calculated acc. to (8). Table II shows the maximum (max) and mean (\emptyset) errors for the reconstruction with both models for each device. It should be remarked that the term "maximum error" refers to the maximum absolute value of the relative deviation between the measurement and the reconstruction. The sign in Table II indicates whether it corresponds to a positive or negative error.

5) *Overview of the results:* In Table II, the results for the underfrequency test are provided on the left, those for the overfrequency test on the right. Results for the range

TABLE II
QUANTITATIVE EVALUATION OF THE RECONSTRUCTION ERROR (%) IN THE DYNAMIC VERIFICATION TEST; V: VACUUM CLEANER, M: MICROWAVE OVEN, L: LED TV SCREEN, F: FAN.

		Underfrequency test (44–50 Hz)								Overfrequency test (50–56 Hz)									
		Range 49–50 Hz				Range 44–50 Hz				Range 50–51 Hz				Range 50–56 Hz					
		P_0^*/Q_0^*	Exponential		Linear		Exponential		Linear		P_0^*/Q_0^*	Exponential		Linear		Exponential		Linear	
			max	∅	max	∅	max	∅	max	∅		max	∅	max	∅	max	∅	max	∅
Active power	V	413 W	+0.48	+0.14	+0.42	+0.11	+8.39	+3.29	+4.71	+2.04	417 W	-0.76	-0.35	-0.79	-0.38	-2.29	-1.53	-6.00	-2.77
	M	1111 W	-0.22	-0.15	-0.22	-0.15	-5.13	-1.13	-5.60	-1.29	1137 W	+0.25	+0.12	+0.25	+0.12	-4.01	-1.44	-4.33	-1.56
	L	172 W	+0.26	+0.05	*	*	+0.34	+0.06	*	*	172 W	+0.25	+0.02	*	*	+0.28	+0.05	*	*
	F	118 W	-0.93	-0.29	-0.94	-0.29	-13.41	-5.49	-13.98	-5.68	117 W	+0.74	+0.42	+0.73	+0.41	+5.68	+2.91	+5.20	+2.75
Reactive power	V	427 var	+0.46	+0.18	+0.46	+0.17	+7.38	+3.01	+6.93	+2.85	429 var	-0.57	-0.19	-0.56	-0.19	-3.61	-1.92	-3.98	-2.05
	M	417 var	-3.19	-1.50	-3.43	-1.53	-35.06	-15.02	-40.06	-17.15	447 var	-0.65	-0.32	-0.91	-0.42	-31.74	-12.34	-39.09	-15.13
	L	64 var	-0.30	-0.17	-0.30	-0.17	-2.34	-1.04	-2.21	-0.99	64 var	+0.38	+0.17	+0.38	+0.17	+1.04	+0.55	+1.14	+0.59
	F	4 var	-	-	-	-	-	-	-	-	4 var	-	-	-	-	-	-	-	-

* Same result as for the reconstruction with the exponential model, since K_{pf} is equal to zero, see Fig. 6.

50±1 Hz are displayed with a gray background. In this range, the maximum errors remain below ±1% for the reconstruction of the active power profiles (upper part of the table). Differences between the exponential and the linear load model reconstruction errors exist only in the second decimal place. For the reactive power reconstruction (lower part of the table), the maximum and mean errors tend to be slightly higher, but remain below ±3.5% and ±1.6%, respectively.

For the underfrequency test, the results in Table II can be visually verified by Fig. 7 (active power) and Fig. 8 (reactive power). We can observe that at the beginning of the first ramp, the reconstructed profiles based on the exponential and the linear model follow the measured behavior quite well. However, except from the active power profiles of the LED TV screen (L , second-lowest plot in Fig. 7), the measured and the reconstructed power profiles tend to diverge beyond the range 49–50 Hz. This phenomena is reflected in the maximum and mean reconstruction errors provided in Table II, where results for the range 50±6 Hz are displayed with a white background. The maximum and mean errors increase approx. by 3 to 40 times compared to those calculated in the range 50±1 Hz. It should be remarked that in most cases from Table II, the reconstruction with the exponential model yields lower errors than the reconstruction with the linear model, with differences of approx. 0.3 to 7 percentage points. Two notable exceptions are the active power reconstruction of the fan during the overfrequency test, and the active power reconstruction of the vacuum cleaner during the underfrequency test (see Fig. 7, V).

C. Steady-State Verification Test Results

To assess the effectiveness of the identified models in computing steady-state power-to-frequency relationship in the wider frequency range (50±6 Hz), we present results from the steady-state verification test in this section. The test was performed with the same representative devices as the dynamic verification test (see previous section).

It should be noted that the appliances were turned off when changing from one steady-state frequency deviation step to another. As mentioned in Section II-C, each step lasted 90 s. To reduce the effects of startup behavior, we only used the measurement data from the last 30 s for the analysis presented

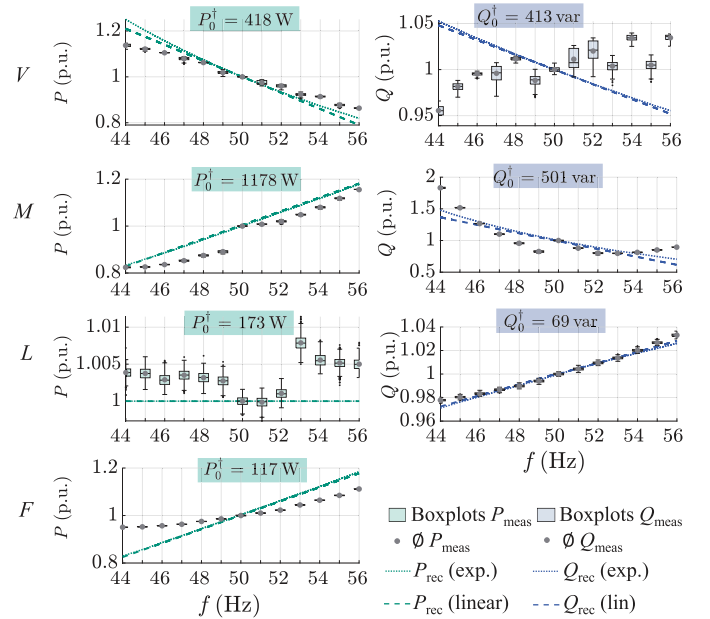


Fig. 9. Measured steady-state active (left) and reactive (power), compared to power computed by the models.

in this section. This data is visualized as boxplots in Fig. 9. The resulting average steady-state power consumption is plotted as a gray dot for each frequency step. To be consistent with Fig. 7 and Fig. 8, power values are shown in per unit in Fig. 9. The new reference values $P_0^†$ and $Q_0^†$ refer to average active and reactive power measured during the 50 Hz step. For the same reason as in the dynamic verification test (see Section IV-B), no reactive power plot is provided for the fan.

The power-to-frequency relationship computed by the models is shown as dotted and dashed lines for the exponential and the linear model, respectively. A first visual comparison suggests that the models successfully reconstruct the measured general patterns in steady-state frequency dependency—in all cases except the reactive power consumption of the vacuum cleaner. In that case, however, it should be remarked that both Fig. 8 (V , second plot) and the extension of the boxplots in Fig. 9 (V , right, first plot) demonstrate that the behavior of the device was quite inconsistent during the test repetitions.

In the next section, we will compare and discuss the findings from the dynamic and steady-state verification test more extensively.

D. Discussion of the Results

Fig. 10 illustrates how the reconstruction error varies with frequency. The figure compares the results from all four selected devices and from both types of verification tests. Results corresponding to the same device are plotted in the same color. It should be noted that the dynamic verification test results (dotted and dashed lines) correspond to those summarized in Table II. The steady-state verification test results (thicker dots and x-symbols at discrete frequency steps) show the reconstruction error based on the measured average steady-state power consumption. On the right side, we provide a zoom-in to the range 50 ± 1 Hz.

It is interesting to note that, except for the case of the microwave (M), the relationship between the reconstruction error and frequency follows the same pattern, both for active (upper plot) and reactive power (lower plot). The more the frequency deviates from 50 Hz, the more increases the reconstruction error. In the range ± 1 Hz, the reconstructed behavior is close to the measured behavior, with errors remaining below $\pm 2\%$ in case of active power, and between -4% to 1% for the reactive power. This finding indicates that identifying the load models with the perturbation-based method is effective for the range of the perturbation signal. Hence, the method may be considered validated. However, as visualized by Fig. 10, the reconstruction with the same load models results in significantly greater errors outside the range 50 ± 1 Hz.

It should be emphasized that the results presented in this work do not allow for drawing conclusions with respect to the general suitability of commonly used exponential and linear frequency-dependent load models to describe load behavior over a wider frequency range. Nonetheless, the results provide valuable insights into challenges that arise in experimentally assessing load models of individual appliances. As mentioned in Section IV-C, the reactive power behavior of the vacuum cleaner in particular demonstrates that the load behavior can be quite inconsistent during test repetitions. A potential way to overcome this issue would be averaging results by a time-consuming increase in test repetitions.

For the other three appliances, the results suggest that K_{pf} and K_{qf} values identified with a 50 ± 1 Hz perturbation signal may not be the most effective model parameters for approximating load behavior in a wider frequency range. Possible methods to be evaluated in future research include using a disturbance signal of a wider amplitude, or a variety of sensitivity values across different frequency ranges.

V. FREQUENCY-DEPENDENT BEHAVIOR OF A PV INVERTER

As mentioned in Section I, PV and battery storage systems installed in Germany need to follow certain grid connection requirements. These requirements are defined in the Application Rule "Power Generating Plants in the Low

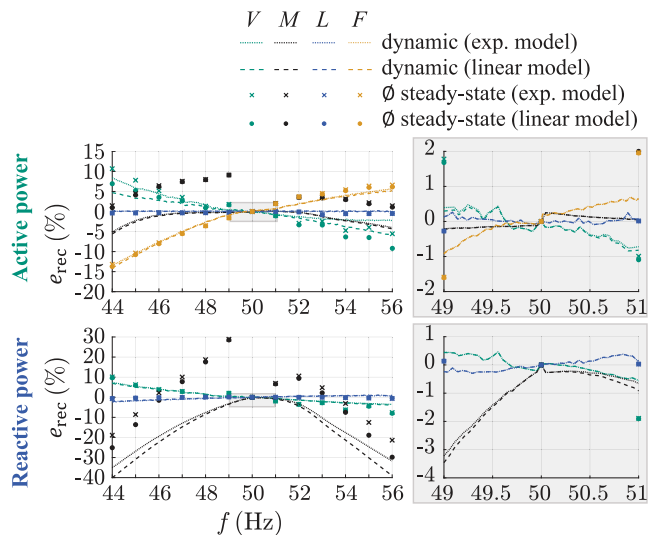


Fig. 10. Comparison of dynamic and average steady-state reconstruction errors.

Voltage Network (VDE-AR-N 4105)" [29], an implementation of the European Network Code *Requirements for Generators* for interconnected systems. This section first summarizes the power adjustment requirements to be followed during grid frequency excursions (Section V-A). Section V-B presents experimental results obtained from testing a real inverter for compliance with these rules. The final Section V-C discusses potential challenges in modeling the behavior in a wider frequency range.

A. Requirements in VDE-AR-N 4105

Frequency-dependent power adjustment rules are only specified for active power. When the frequency is outside the range 50 ± 0.2 Hz, the grid situation in the Continental Europe power system is considered critical. As illustrated by Fig. 11, PV and storage systems are required to actively adjust their active power setpoint during these over- or underfrequency situations. The response delay time Δt_{del} should be "below two seconds, if possible" [29].

1) *Overfrequency situation:* Overfrequency situations represent a generation surplus in the system. To counteract this situation, PV and battery storage systems are required to decrease their active power feed-in according to a droop function. In the absence of any specific request from the grid operator, the gradient is defined as -40% of P_{ref} per hertz. For PV systems, P_{ref} refers to the active power at the moment that the frequency reaches 50.2 Hz.

2) *Underfrequency situation:* Underfrequency situations represent a load surplus in the system. Usually, PV systems are not being curtailed during normal operation, which is why a further increase of the active power fed into the grid is technically impossible. Such behavior is only required for battery storage systems (see Fig. 11) [29].

B. Investigation of the Behavior of an Inverter

In addition to the domestic devices listed in Table I, a real PV inverter was selected as load under test. To achieve

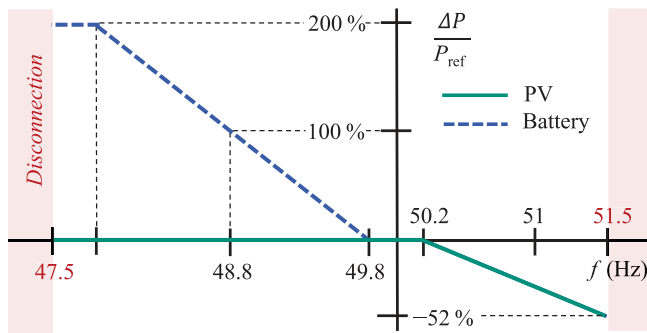


Fig. 11. Droop requirements defined in VDE-AR-N 4105 [29], based on [18].

TABLE III
PV INVERTER SETUP UNDER TEST.

PV inverter	Inverter model	SMA Mini Central SMC 7000HV
	Nominal AC power	6.65 kVA
	Connection	Single-phase
	Nominal frequency	50 or 60 Hz
	Permissible frequency range	-6/+5 Hz of the nominal value
PV emulator	DC source	ET System Lab/SMS31000

maximum repeatability in the tests, it was connected to a PV emulator instead of real PV panels. Information on the nominal data of the inverter and the emulator is provided in Table III. The aim of the tests performed with this exemplary inverter system was to demonstrate how currently defined grid code requirements impact the frequency-dependent behavior of such modern residential loads.

To test for compliance with VDE-AR-N 4105, the inverter was exposed to five types of trapezoidal frequency variations. The top value was 51 or 51.6 Hz, and the RoCoF during the ramps varied from ± 0.03 Hz/s to ± 2 Hz/s. Each trapezoidal variation was repeated three times. Fig. 12 shows the example of the ± 0.03 Hz/s experiment. During each repetition of the rising ramp, the same behavior can be observed. When the frequency is in the range 50 to 50.2 Hz, the inverter feeds approx. $P_{ref} \approx 1230$ W into the grid. Since the inverter performs Maximum Power Point tracking in this normal uncurtailed mode, a power fluctuation of about 200 W can be observed. It is interesting to note that this power fluctuation stops when the frequency surpasses 50.2 Hz. As required by VDE-AR-N 4105 (see Fig. 11), the inverter then gradually reduces the power fed into the grid in a controlled manner, based on the power P_{ref} measured at the moment the frequency reaches 50.2 Hz. When the frequency reaches 51.5 Hz, the inverter disconnects from the grid, which is why the power measured in Fig. 12 (bottom plot) decreases to zero. Before the inverter disconnects, the overall power adjustment ΔP reaches approx. 490 W during this frequency increase of 1.5 Hz. This corresponds to a change of approx. -40% of P_{ref} per hertz, which is in accordance with the droop requirements described in Fig. 11.

The zoom-in plot in Fig. 12 (right) allows us to obtain a closer look at the inverter's power adjustment behavior during the second frequency rise (marked with a gray background in the left plot). The value 50.2 Hz is reached at time $t = 249$ s.

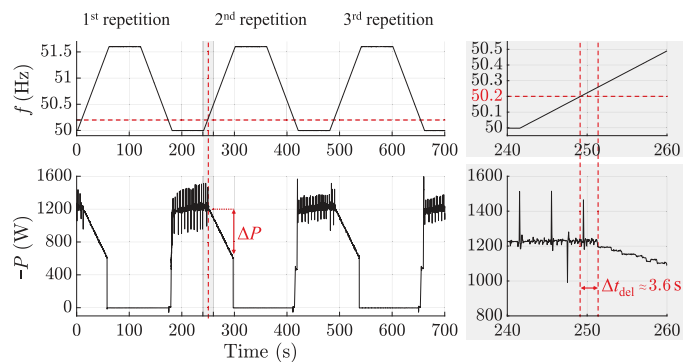


Fig. 12. PV inverter overfrequency behavior (power adjustment with delay and eventual disconnection at 51.5 Hz); zoom-in to the gray area on the right.

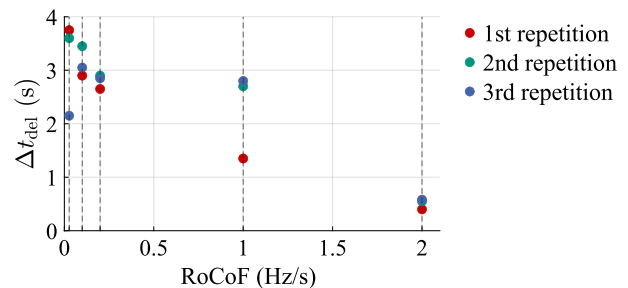


Fig. 13. Measured response delay times Δt_{del} for power adjustment, for frequency ramps of five different RoCoF values (0.03 Hz/s, 0.1 Hz/s, 0.2 Hz/s, 1 Hz/s and 2 Hz/s).

There is a delay Δt_{del} of approx. 3.6 s until the inverter actually starts to decrease the power fed into the grid.

It should be emphasized that we found the delay to vary with each test. For the three repetitions shown in Fig. 12, Δt_{del} was 3.8 s, 3.6 s and 2.2 s. In Fig. 13, we compare these values to those measured for disturbances with different RoCoF values. The results shown in Fig. 13 suggest that the delay tends to be higher with slower frequency rises.

C. Discussion of the Results

According to the data sheet information summarized in Table III, it is technically possible to operate the inverter in the range 44–55 Hz. This corresponds with generator withstand capability requirements defined in some isolated European power systems (see Section I). For the case of the German inverter market, it should be mentioned that not all manufacturers specify their inverter models to operate in the range that would be required for isolated systems. Some are only specified for the range 47–53 Hz [18]. However, it is likely that the frequency-dependent behavior of most inverters can be altered within the range defined in the technical specifications through minor parameter modifications or software updates. In [18], it was demonstrated for another SMA inverter that settings such as the tripping values (normally 47.5 Hz and 51.5 Hz, see Fig. 11) or the starting frequency for overfrequency power adjustment (normally 50.2 Hz) can be modified via Modbus. However, it did not appear possible to change the response delay time characteristics to be different from Fig. 13.

These findings imply that commonly used load models (see Section II-A) may not be suitable for describing the behavior of PV inverters in a wider frequency range. The results in Section IV confirm that conventional domestic loads tend to react immediately to frequency changes. In contrast, the power adjustment delay in the range of seconds that we observed for the inverter can be considered non-negligible. It should further be noted that the varying nature of the delay makes it challenging to accurately predict the behavior of individual inverters. This topic can be an interesting area for future work, especially when it comes to the characterization of aggregated residential loads of different types.

VI. CONCLUSION

In this paper, we presented an experimental investigation into the frequency dependency of residential loads. For sixteen domestic appliances, updated frequency sensitivity values under realistic test conditions were obtained with the novel perturbation-based approach in the range 50 ± 1 Hz. The identified sensitivity values K_{pf} and K_{qf} can be used as parameters for the exponential and the linear frequency-dependent load model which are commonly used in power system studies. To assess and verify these models, four representative appliances were exposed to dynamic and steady-state frequency disturbances in the extended range 50 ± 6 Hz. Upon comparing the measured actual load behavior with the behavior computed by the models, it was found that the power reconstruction error significantly rises beyond the 50 ± 1 Hz range. This result indicates that model parameters identified for a small frequency range may not be most effective for predicting the behavior during larger frequency variations. In this paper, the loads under tests also included a PV inverter, representative of today's distributed in-house generator and storage systems. During frequency disturbances, these systems are required to actively adjust their active power setpoint. However, the experimental results obtained from the PV inverter show that this power adjustment is not immediate, but comes with a varying response delay time. Therefore, commonly used load models are not suitable for describing the behavior of such systems.

REFERENCES

- [1] ENTSO-E SPD – Inertia TF, “Inertia and Rate of Change of Frequency (RoCoF) - Version 17,” Technical Report, 2020.
- [2] M. L. Little, S. F. Rabbi, K. Pope, and J. E. Quaioco, “Unified Probabilistic Modeling of Wind Reserves for Demand Response and Frequency Regulation in Islanded Microgrids,” *IEEE Transactions on Industry Applications*, vol. 54, no. 6, pp. 5671–5681, 2018.
- [3] S. Bruno, G. Giannoccaro, C. Iurlaro, M. L. Scala, M. Menga, C. Rodio, and R. Sbrizzai, “Fast Frequency Support Through LED Street Lighting in Small Non-Synchronous Power Systems,” *IEEE Transactions on Industry Applications*, vol. 59, no. 2, pp. 2277–2287, 2023.
- [4] DIN EN 50160, Voltage characteristics of electricity supplied by public electricity networks; German version EN 50160:2010 + Cor.:2010 + A1:2015 + A2:2019 + A3:2019.
- [5] J. Geis-Schroer, M. Suriyah, and T. Leibfried, “Frequency Fluctuations in European Isolated Systems: A Review on Standards, Available Recordings and Grid Code Requirements,” in *2023 58th International Universities Power Engineering Conference (UPEC)*, pp. 1–6, 2023.
- [6] H. A. Bauman, O. W. Manz, J. E. McCormack, and H. B. Seeley, “System load swings,” *Electrical Engineering*, vol. 60, no. 6, pp. 541–546, 1941.

- [7] J. M. Comly, C. B. Kelley, J. E. McCormack, H. W. Phillips, and T. W. Schroeder, “Emergency control of system loads,” *Trans. of the American Institute of Electrical Engineers*, vol. 67, no. 2, pp. 1474–1483, 1948.
- [8] M. S. Chen, “Determining load characteristics for transient performances. Volume 3. Procedure for modeling power system loads. Final report. [DSAP computer code],” 5 1979.
- [9] G. De Carne, S. Bruno, M. Liserre, and M. La Scala, “Distributed Online Load Sensitivity Identification by Smart Transformer and Industrial Metering,” *IEEE Transactions on Industry Applications*, vol. 55, no. 6, pp. 7328–7337, 2019.
- [10] A. Bokhari *et al.*, “Experimental Determination of the ZIP Coefficients for Modern Residential, Commercial, and Industrial Loads,” *IEEE Transactions on Power Delivery*, vol. 29, no. 3, pp. 1372–1381, 2014.
- [11] J. V. Milanovic, K. Yamashita, S. M. Villanueva, S. Ž. Djokic, and L. M. Korunović, “International industry practice on power system load modeling,” *IEEE Transactions on Power Systems*, vol. 28, no. 3, pp. 3038–3046, 2013.
- [12] A. Arif, Z. Wang, J. Wang, B. Mather, H. Bashualdo, and D. Zhao, “Load modeling—a review,” *IEEE Transactions on Smart Grid*, vol. 9, no. 6, pp. 5986–5999, 2018.
- [13] M. Andresen, G. De Carne, and M. Liserre, “Load-dependent active thermal control of grid-forming converters,” *IEEE Transactions on Industry Applications*, vol. 56, no. 2, pp. 2078–2086, 2020.
- [14] S. M. H. Rizvi, S. K. Sadanandan, and A. K. Srivastava, “Real-Time ZIP Load Parameter Tracking Using Sensitivity-Based Adaptive Window and Variable Elimination With Realistic Synchrophasor Data,” *IEEE Trans. on Industry Applications*, vol. 57, no. 6, pp. 6525–6536, 2021.
- [15] “IEEE Guide for Load Modeling and Simulations for Power Systems,” *IEEE Std 2781-2022*, pp. 1–88, 2022.
- [16] The Regulatory Assistance Project (RAP), “Report on the German power system.” Version 1.2 Study commissioned by Agora Energiewende. 2015. [Online] www.agora-energiewende.de (acc.: 30/11/2023).
- [17] 50hertz, Amprion, TenneT, and Transnet BW, “EEG-Anlagenstammdaten zur Jahresabrechnung 2021 [Renewable Energy Sources Act (EEG) plant data for annual billing 2021].” 2022. [Online] <https://www.netztransparenz.de/EEG/Anlagenstammdaten> (acc.: 13/01/2022).
- [18] J. Geis-Schroer, G. Bock, M. Suriyah, and T. Leibfried, “Impact of changing frequency standards on grid-connected PV and battery systems in the German low voltage system,” in *27th International Conference on Electricity Distribution (CIRED 2023)*, vol. 2023, pp. 3342–3346, 2023.
- [19] Q. Tao *et al.*, “The Potential of Frequency-Based Power Control in Distribution Grids,” in *2022 IEEE 13th Int. Symposium on Power Electronics for Distributed Generation Systems (PEDG)*, pp. 1–6, 2022.
- [20] F. Wald, Q. Tao, and G. De Carne, “Virtual Synchronous Machine Control for Asynchronous Grid Connections,” *IEEE Transactions on Power Delivery*, vol. 39, no. 1, pp. 397–406, 2024.
- [21] L. Hajagos and B. Danai, “Laboratory measurements and models of modern loads and their effect on voltage stability studies,” *IEEE Transactions on Power Systems*, vol. 13, no. 2, pp. 584–592, 1998.
- [22] J. Milanovic *et al.*, “CIGRE WG C4.605 : “Modelling and aggregation of loads in flexible power networks.” Technical Brochure 566, 2014.
- [23] L. M. Korunović, J. V. Milanović, S. Z. Djokic, K. Yamashita, S. M. Villanueva, and S. Sterpu, “Recommended parameter values and ranges of most frequently used static load models,” *IEEE Transactions on Power Systems*, vol. 33, no. 6, pp. 5923–5934, 2018.
- [24] C. Concordia and S. Ihara, “Load representation in power system stability studies,” *IEEE Transactions on Power Apparatus and Systems*, vol. PAS-101, no. 4, pp. 969–977, 1982.
- [25] P. Kundur and N. Balu, *Power System Stability and Control*. McGraw-Hill, 1994.
- [26] Q. Tao, J. Geis-Schroer, M. Courcelle, T. Leibfried, and G. D. Carne, “Investigation of Frequency Dependency of Residential Loads in Modern Power Systems: An Experimental Approach,” in *2023 11th International Conference on Power Electronics and ECCE Asia (ICPE 2023 - ECCE Asia)*, pp. 329–334, 2023.
- [27] G. De Carne, M. Liserre, and C. Vournas, “On-Line Load Sensitivity Identification in LV Distribution Grids,” *IEEE Transactions on Power Systems*, vol. 32, no. 2, pp. 1570–1571, 2017.
- [28] S. Kochannek *et al.*, “Establishing a Hardware-in-the-Loop Research Environment with Hybrid Energy Storage System,” in *2016 IEEE PES Conf. on Innovat. Smart Grid Technol. (ISGT-Asia)*, pp. 497–503, 2016.
- [29] Power Generating Plants in the Low Voltage Network (VDE-AR-N 4105). Application Rule. 2018.



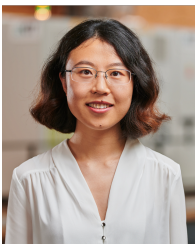
Johanna Geis-Schroer (S'23) received her B.Sc. degree in industrial engineering in 2017, and her M.Sc. degree in electrical engineering in 2020, both from the Karlsruhe Institute of Technology (KIT), Karlsruhe, Germany. In 2019, she spent one semester as a research intern at the Energy Production and Infrastructure Center at the University of North Carolina at Charlotte, North Carolina, USA. Currently, she is pursuing her Ph.D. degree in electrical engineering at KIT, and is working as a research associate at the Institute of Electric Energy

Systems and High-Voltage Technology (IEH) at KIT. Her research interests include frequency dynamics in low-inertia power systems, load modeling, and the impacts of large frequency variations on loads and grid equipment.



Michael Suriyah (M'14) received the Diploma and the M.Sc. degrees in electrical engineering from the Karlsruhe University of Applied Sciences, Karlsruhe, Germany, in 2007 and 2008, respectively, and the Ph.D. degree in electrical engineering from the Karlsruhe Institute of Technology (KIT), Karlsruhe, Germany, in 2013. He is the head of the Department for Power Networks in the Institute of Electric Energy Systems and High-Voltage Technology (IEH) at KIT. His research interests include aging diagnostics and onsite testing

of power transformers, high-voltage testing methods, analysis of electric power networks, and planning of future power systems. He is a member of VDE.



Qiucen Tao (S'22) received her B.Sc. degree from Southeast University, China, in 2017, and her M.Sc. degree from the Karlsruhe Institute of Technology (KIT), Karlsruhe, Germany, in 2021, both in electrical engineering. She is currently pursuing her Ph.D. degree as a member of the "Real-Time Systems for Energy Technologies" Group and the "Energy Lab" at KIT. Her research interests include load sensitivity identification, demand-side management, smart distribution networks, and the real-time simulation and power hardware in the loop

implementation of these systems.



Thomas Leibfried (M'96, SM'20) received the Dipl.-Ing. and Dr.-Ing. degrees in electrical engineering from the University of Stuttgart, Stuttgart, Germany, in 1990 and 1996, respectively. From 1996 to 2002, he was with Siemens AG, Nuremberg, Germany, working in the power transformer business in various technical and management positions. In 2002, he joined the University of Karlsruhe (now Karlsruhe Institute of Technology, KIT), Karlsruhe, Germany, as the head of the Institute of Electric Energy Systems and

High-Voltage Technology (IEH). From 2014 to 2018 he served as Dean of his faculty. In 2024, he was elected as member of the scientific council "Electrical Engineering and Information Technology" within the German research foundation for the period 2024-2028. His research interests are power electronic applications in the power grid, stability of grids with high power electronic penetration and high-voltage technology. He is a member of VDE and CIGRE.



Maëva Courcelle (S'22) received her M.Sc. degree equivalent (Diplôme d'Ingénieur) from Telecom Physique Strasbourg, Illkirch-Graffenstaden, France, in 2021. During her general engineering studies majoring in electronics and embedded systems, she deepened her knowledge in power electronics as an exchange student at the Karlsruhe Institute of Technology (KIT), Karlsruhe, Germany. Since the end of 2021, she has been pursuing a Ph.D. degree as part of the "Real-Time Systems for Energy Technologies" Group and the "Energy Lab" at KIT.

In 2023, she spent one semester as a visiting researcher at the FREEDM Systems Center at North Carolina State University, USA. Her research interests include real-time load parameter identification for the modeling and control of distribution networks.



Giovanni De Carne (S'14, M'17, SM'21) received the B.Sc. and M.Sc. degrees in electrical Engineering from the Polytechnic University of Bari, Italy, in 2011 and 2013, respectively, and the Ph.D. degree from the Chair of Power Electronics, Kiel University, Germany, in 2018. Prof. De Carne is currently W3 (full) professor at the Institute for Technical Physics at the Karlsruhe Institute of Technology, Karlsruhe, Germany, where he leads the "Real Time Systems for Energy Technologies" Group and the "Power Hardware In the Loop Lab".

He is currently supervising PhD students, managing academic and industrial projects, and developing multi-MW power hardware in the loop testing infrastructures for energy storage systems and hydrogen-based drives. He has authored/coauthored more than 100 peer-reviewed scientific papers. His research interests include power electronics integration in power systems, solid state transformers, real time modelling, and power hardware in the loop. Prof. De Carne successfully hosted the IEEE eGrid2023 Workshop in Karlsruhe in October 2023 with high participation from industry. He has been technical program committee chair for several IEEE conferences, associate editor of the IEEE Open Journal of Power Electronics and several other IEEE and IET journals.



Gregor Bock received his B.Sc. degree in electrical engineering from the Karlsruhe Institute of Technology (KIT), Karlsruhe, Germany, in 2022, where he is currently pursuing a M. Sc. degree with a specialization in renewable energies and power electronics. He is also working as a student research assistant at KIT. His research interests include high-power converter systems for grid interconnections and the large-scale deployment of renewable energy sources.